EDITOR'S CHOICE

Use of multiplex PCR and real-time PCR to detect human herpes virus genome in ocular fluids of patients with uveitis

S Sugita,[1] N Shimizu,[2] K Watanabe,[2] M Mizukami,[3] T Morio,[3] Y Sugamoto,[1] M Mochizuki[1]

[1] Department of Ophthalmology & Visual Science, Medical Research Institute, Tokyo Medical and Dental University, Tokyo, Japan; [2] Department of Virology, Medical Research Institute, Tokyo Medical and Dental University, Tokyo, Japan; [3] Center for Cell Therapy, Tokyo Medical and Dental University, Tokyo, Japan

Correspondence to: Professor M Mochizuki, Department of Ophthalmology & Visual Science, Tokyo Medical and Dental University Graduate School of Medicine, 1-5-45 Yushima, Bunkyo-ku, Tokyo 113-8519, Japan; m.manabu.oph@tmd.ac.jp

Accepted 17 February 2008
Published Online First 11 April 2008

ABSTRACT

Aim: To measure the genomic DNA of human herpes viruses (HHV) in the ocular fluids and to analyse the clinical relevance of HHV in uveitis.

Methods: After informed consent was obtained, a total of 111 ocular fluid samples (68 aqueous humour and 43 vitreous fluid samples) were collected from 100 patients with uveitis. The samples were assayed for HHV-DNA (HHV1–8) by using two different polymerase chain reaction (PCR) assays, qualitative PCR (multiplex PCR) and quantitative PCR (real-time PCR).

Results: In all of the patients with acute retinal necrosis (n = 16) that were tested, either the HSV1 (n = 2), HSV2 (n = 3), or VZV (n = 11) genome was detected. In all patients, high copy numbers of the viral DNA were also noted, indicating the presence of viral replication. In another 10 patients with anterior uveitis with iris atrophy, the VZV genome was detected. When using multiplex PCR, EBV-DNA was detected in 19 of 111 samples (17%). However, real-time PCR analysis of EBV-DNA indicated that there were only six of the 19 samples that had significantly high copy numbers. The cytomegalovirus (CMV) genome was detected in three patients with anterior uveitis of immunocompetent patients and in one immunocompromised CMV retinitis patient. In addition, one patient with severe unilateral panuveitis had a high copy number of HHV6-DNA. There was no HHV7- or HHV8-DNA detected in any of the samples.

Conclusions: A qualitative multiplex PCR is useful in the screening of viral infections. However, the clinical relevance of the virus infection needs to be evaluated by quantitative real-time PCR.

Human herpes virus (HHV) affects various ocular tissues and is known to cause anterior and/or posterior uveitis, which is characterised by mutton-fat keratic precipitates (KPs), ocular hypertension, iris atrophy, vitreous opacity, and necrotic retinitis. Using polymerase chain reaction (PCR), previous studies have demonstrated the presence of genomic DNA for HHV in the aqueous humour and vitreous fluids in patients with herpetic uveitis, including herpetic keratouveitis, herpes zoster ophthalmicus, zoster sine herpete, acute retinal necrosis, and cytomegalovirus retinitis.[1–7] With recent advances in molecular biology, use of real-time PCR now makes it possible for quantitative measurements of the viral load associated with herpes virus diseases in the eye.[5 6] In addition, multiplex qualitative PCR has the advantage of combining several different primer pairs in the same amplification reaction with the net result of producing different specific virus-amplicons in ocular infectious diseases.[7] Therefore, multiplex PCR can be used to detect the presence of viruses within samples.

In this study, we collected ocular samples from various uveitis patients and then tried to detect the HHV genome when using combinations of two PCR systems: (1) multiplex qualitative PCR and (2) real-time quantitative PCR.

MATERIAL AND METHODS

Subjects

Samples of aqueous humour (n = 68) and vitreous fluid (n = 43) were collected from 100 patients with uveitis and ocular lymphoma. Underlying pathology comprised herpetic keratouveitis (n = 7), herpetic anterior uveitis/iridocyclitis (n = 16), acute retinal necrosis (ARN; n = 16), cytomegalovirus (CMV) retinitis (n = 1), human T lymphotropic virus type 1 (HTLV-1) uveitis (n = 1), ocular toxoplasmosis (n = 2), scleritis (n = 3), ocular sarcoidosis (n = 7), Vogt–Koyanagi–Harada (VKH) disease (n = 2), Behçet disease (n = 2), idiopathic uveitis (n = 26) and intraocular lymphoma (n = 12). At the time of sampling, uveitis patients displayed active intraocular inflammation.

An aliquot of 0.1 ml of the aqueous humour was aspirated with a 30 G needle. In patients with uveitis who were undergoing vitreous surgery, non-diluted vitreous fluid samples were collected from the patients during surgery (diagnostic pars-plana vitrectomy). The samples used in this study were collected between 1999 and 2007.

Polymerase chain reaction

Genomic DNA of HHV in the aqueous humour and vitreous fluids was measured through the use of two independent PCR assays: (1) a qualitative multiplex PCR and (2) a quantitative real-time PCR. The result analysis for the PCR is shown in fig 1.

DNA was extracted from samples using an E21 virus minikit (Qiagen, Valencia, CA) installed on a Robotic workstation for automated purification of nucleic acids (BioRobot E21, Qiagen). The multiplex PCR was designed to qualitatively measure genomic DNA of eight human herpes viruses, that is, herpes simplex virus type 1 (HSV-1), type 2 (HSV-2), Varicella-zoster virus (VZV), Epstein–Barr virus (EBV), cytomegalovirus (CMV), human herpes virus type 6 (HHV6), type 7 (HHV7) and type 8 (HHV8). The PCR was performed using a

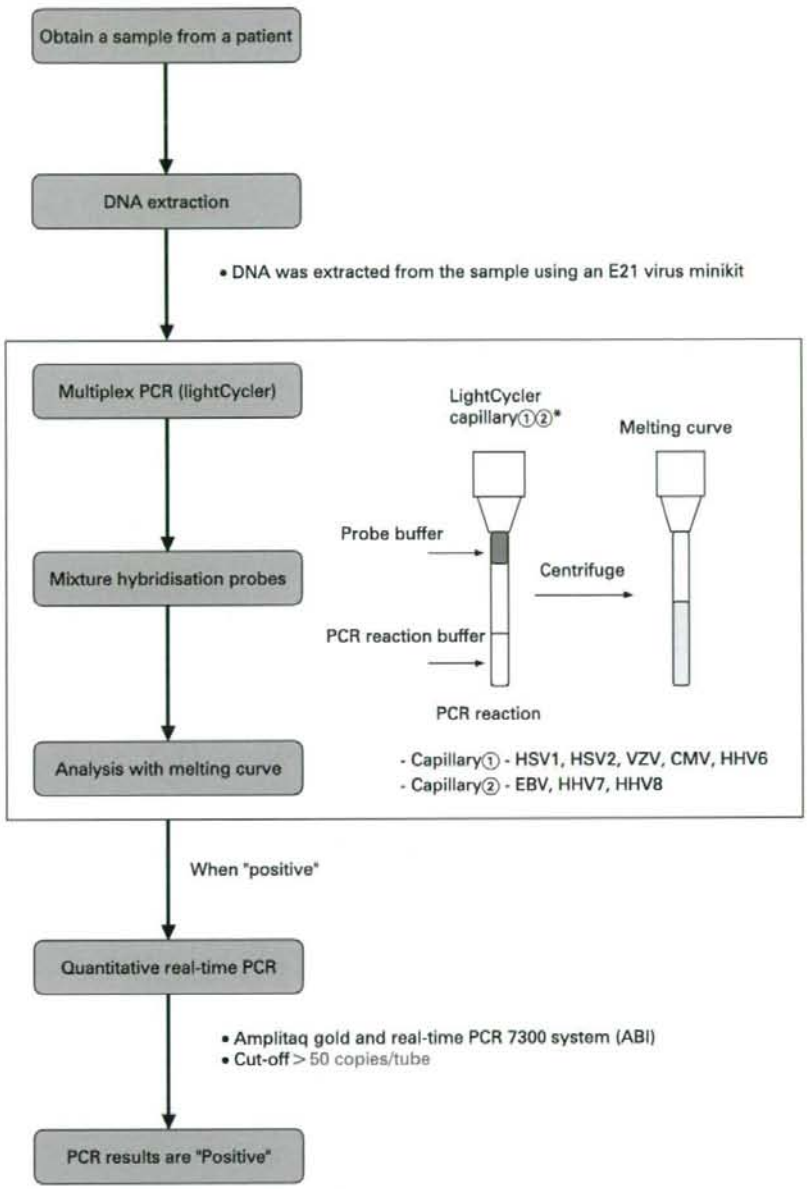

Figure 1 Use of multiplex PCR and real-time PCR for the analysis of human herpes virus family genomic DNA in ocular fluids of patients with uveitis. We performed independent PCR methods to detect herpes viruses, using both a qualitative multiplex PCR and a quantitative real-time PCR. After DNA extraction from each of the samples, multiplex PCR was performed to screen from HHV1 to HHV8 using two LightCycler capillaries. When a "positive" result was observed, real-time PCR was performed to measure the viral load. When more than 50 copies/tube (5×10^3/ml) were observed, the value was considered to be significant. CMV, cytomegalovirus; EBV, Epstein–Barr virus; HHV, human herpes virus; HSV, herpes simplex virus; VZV, Varicella-zoster virus.

LightCycler (Roche, Switzerland). Primers and probes of HHV1–8 and the PCR conditions have been described previously.[8] Specific primers for the virus were used with Accuprime Taq (Invitrogen, Carlsbad, CA). Products were subjected to 40 cycles of PCR amplification. Hybridisation probes were then mixed with the PCR products. Subsequently, real-time PCR was performed only for the human herpes virus, with the genomic DNA detected by multiplex PCR (fig 1). The real-time PCR was performed using Amplitaq Gold and the Real-Time PCR 7300 system (ABI, Foster City, CA). The sequence of the HHV1–8 primers and probes are shown in table 1. The primers of the viruses and the PCR conditions have been described in previous reports.[9–13] Our research group has also previously reported the primers of the sequences for VZV.[14] All of the products obtained were subjected to 45 cycles of PCR amplification. The value of viral copy number in the sample was considered to be significant, when more than 50 copies/tube (5×10^3/ml) were observed.

RESULTS

Our initial PCR results indicated HHV positivity in the ocular fluids of uveitis patients. As shown in table 2, multiplex PCR detected seven patients with HSV1-DNA while real-time PCR found that all seven of these patients also had a high HSV1 viral load. In addition, HSV2-DNA was detected in three patients, with all of these patients having a high viral load. In 29 patients,

Table 1 Sequence for primers and probes in human herpes viruses (HHV) using real-time PCR

Herpes virus	Sequence for primers and probes	Amplification
HSV1 and 2	HSV-F: CGCATCAAGACCACCTCCTC	gB
	HSV-R: GCTCGCACCACGCGA	
	HSV1-P: JOE-TGGCAACGCGGCCCAAC-TAMRA	
	HSV2-P: FAM-CGGCGATGCGCCCCAG-TAMRA	
VZV	VZV-F: AACTTTTACATCCAGCCTGGCG	ORF29
	VZV-R: GAAAACCCAAACCGTTCTCGAG	
	VZV-P: FAM-TGTCTTTCACGGAGGCAAACACGT-TAMRA	
EBV	EBV-F: CGGAAGCCCTCTGGACTTC	BALF5
	EBV-R: CCCTGTTTATCCGATGGAATG	
	EBV-P: FAM-TGTACACGCACGAGAAATGCGCC-TAMRA	
CMV	CMV-F: CATGAAGGTCTTTGCCCAGTAC	IE-1
	CMV-R: GGCCAAAGTGTAGGCTACAATAG	
	CMV-P: FAM-TGGCCCGTAGGTCATCCACACTAGG-TAMRA	
HHV6	HHV6-F: GACAATCACATGCCTGGATAATG	U65-U66
	HHV6-R: TGTAAGCGTGTGGTAATGTACTAA	
	HHV6-P: FAM-AGCAGCTGGCGAAAAGTGCTGTGC-TAMRA	
HHV7	HHV7-F: CGGAAGTCACTGGAGTAATGACAA	U37
	HHV7-R: CCAATCCTTCCGAAACCGAT	
	HHV7-P: FAM-CTCGCAGATTGCTTGTTGGCCATG-TAMRA	
HHV8	HHV8-F: CCTCTGGTCCCCATTCATTG	ORF65
	HHV8-R: CGTTTCCGTCGTGGATGAG	
	HHV8-P: FAM-CCGGCGTCAGACATTCTCACAACC-TAMRA	

The real-time herpes simplex virus (HSV) PCR is a multiplexing PCR that can detect both HSV1 and HSV2 DNA in the same reaction. The optimised gB primer pairs amplify both HSV1 and 2 with equal efficiency, with the two type-specific probes labelled with different fluorescent dyes. HSV1 probe is labelled with JOE at the 5'-end and with TAMRA at the 3'-end. HSV2 probe is labelled with FAM at the 5'-end and with TAMRA at the 3'-end.
CMV, cytomegalovirus; EBV, Epstein–Barr virus; VZV, Varicella-zoster virus.

VZV-DNA was detected, but only 21 patients (72%) had a high viral load. EBV was detected in 19 patients, but only six out of the 19 cases were positive (32%). CMV-DNA was detected in six patients, with four out of the six cases (67%) found to be positive by the real-time PCR. HHV6-DNA was detected in only one patient by both of the PCR methods. There were no patients for which HHV7 and HHV8 were detected. Overall, there were 65 multiplex PCR positive patients and 42 real-time PCR positive patients (table 2). Clinically, we decided that only if HHV-DNA could be detected in a sample (aqueous humour and/or vitreous) by both PCR methods would the patient then be considered to be positive. If a patient was found to be positive by only one of the PCR methods, for example, positive by multiplex qualitative PCR and negative (<50 copies/tube) by real-time quantitative PCR, we did not take this as PCR-positive (fig 1).

Table 2 Human herpes virus-PCR positivity in ocular fluids of 100 patients with uveitis

Herpes virus	Multiplex PCR	Real-time PCR
HSV1	7/100 (7%)	7/7 (100%)
HSV2	3/100 (3%)	3/3 (100%)
VZV	29/100 (29%)	21/29 (72%)
EBV	19/100 (19%)	6/19 (32%)
CMV	6/100 (6%)	4/6 (67%)
HHV6	1/100 (1%)	1/1 (100%)
HHV7	0/100 (0%)	–
HHV8	0/100 (0%)	–
Total	65/100 (65%)	42/65 (65%)

Qualitative multiplex PCR was performed in order to screen for and detect human herpes virus (HHV) genomic DNA, HHV1–HHV8. When the genomic DNA was detected by the multiplex PCR (n = 65), real-time PCR was then performed only for the HHV.
CMV, cytomegalovirus; EBV, Epstein–Barr virus; HSV, herpes simplex virus; VZV, Varicella-zoster virus.

Subsequently, we analysed the results for each the viruses, from HHV1 to HHV8. The summary of the results is shown in table 3. HSV1 was detected in two cases of keratouveitis, and in three cases of anterior uveitis. These patients had mutton-fat KPs, ocular hypertension and anterior chamber cells. HSV1 was also detected in two cases of acute retinal necrosis (ARN). HSV2 was detected in three cases of ARN. VZV was detected in 10 cases of herpetic anterior uveitis and in 11 cases of ARN. During the time after the initial onset of anterior uveitis, iris atrophy developed in these patients. Higher viral load in the aqueous humour was well correlated with tissue damage, such as iris atrophy.[14] In addition, as we have reported previously, real-time PCR of the ocular fluids from ARN patients (n = 16) indicated high viral loads of VZV (n = 11, 69%), HSV1 (n = 2, 12%), and HSV2 (n = 3, 19%).[8]

EBV was detected in only one case of idiopathic uveitis. This patient had acute anterior uveitis with hypopyon and was HLA-B27 negative. Therefore, as previously reported, we diagnosed EBV-related acute anterior uveitis.[15] EBV was also detected in two cases of VZV-associated anterior uveitis and in two cases of VZV-ARN. This suggests that these patients have a high copy number of VZV, as well as EBV in their ocular fluids. EBV was also detected in one case of ocular B-cell lymphoma.

CMV was detected in a case of cytomegalovirus retinitis and in three cases of CMV-associated anterior uveitis. Representative results from the multiplex qualitative PCR can be seen in fig 2. CMV-DNA was detected in the aqueous humour, and quantitative real-time PCR revealed there were 2.3×10^5 copies/mL of CMV-DNA in the specimen. As we previously reported, in the affected eye there were whitish small-size mutton-fat KPs along with mild inflammation in the anterior chamber.[16] During the 8 years this particular patient was followed, he had been considered to have a case of Posner–Schlossman syndrome. This patient had no retinitis, and additionally he was not found to be immunocompromised.

Br J Ophthalmol 2008;**92**:928–932. doi:10.1136/bjo.2007.133967

Table 3 PCR results for each herpes virus genome in patients with uveitis

Herpes virus	Clinical diagnosis	PCR-positive*/total no of patients
HSV1	Herpetic keratouveitis	2/7†
	Herpetic anterior uveitis	3/16
	Acute retinal necrosis	2/16
	Others	0/61
HSV2	Acute retinal necrosis	3/16
	Others	0/84
VZV	Herpetic anterior uveitis	10/16
	Acute retinal necrosis	11/16
	Others	0/68
EBV	Idiopathic uveitis	1/26
	Herpetic anterior uveitis (VZV)	2/16
	Acute retinal necrosis (VZV)	2/16
	Intraocular lymphoma	1/12
	Others	0/30
CMV	Herpetic anterior uveitis	3/16
	Cytomegalovirus retinitis	1/1
	Others	0/83
HHV6	Idiopathic uveitis	1/26
	Others	0/74
HHV7	–	0/100
HHV8	–	0/100

*Detection of HHV-DNA by both multiplex PCR and real-time PCR.
†In the seven patients with keratouveitis, our PCR system detected HSV1-DNA in two patients.
CMV, cytomegalovirus; EBV, Epstein–Barr virus; HHV, human herpes virus; HSV, herpes simplex virus; VZV, Varicella-zoster virus.

A high copy number of HHV6-DNA was detected in only one patient with severe unilateral panuveitis. In this patient, multiple retinal exudates, vitreous opacity, along with a whitish mass lesion were observed in the affected eye. We reported this case as HHV6-associated panuveitis.[17] In the current study, HHV7- or HHV8-DNA was not detected in any of the patients (table 3).

DISCUSSION

Human herpes viruses (HHV) can widely affect the eye and be expressed in ocular tissues or excreted in ocular fluids. Previously, the diagnosis of intraocular HHV infection was made by measuring local production of specific anti-virus antibodies—for example, using the Goldmann–Witmer coefficient. Recently, diagnosis has also been performed through the detection of the virus genome by PCR. Cell-free herpes virus DNA has been detected in the aqueous humour and vitreous fluids of patients with uveitis.[1–7] In the current study, we showed that intraocular HHV-DNA was detectable over a wide range of HHV-associated uveitis when analysis was performed using the two PCR methods. Thus, the current PCR system may be a valuable tool in the diagnosis of infectious uveitis. In addition, with the use of these examinations, this allows non-herpetic uveitis patients to be excluded.

When faced with a clinical situation that suggests a differential diagnosis of HHV1–8, the multiplex PCR assay can provide a rapid and reliable diagnosis, even when only small sample amounts are available for examination in the ocular microbiology laboratory. The majority of the viruses associated with eye diseases are related to the herpes virus group. Therefore, the last decade has seen several studies concluding that herpes virus PCR-based laboratory investigations are valuable tools in the diagnosis of viral diseases of the eye. The advantages of developing the multiplex PCR assay are obvious,

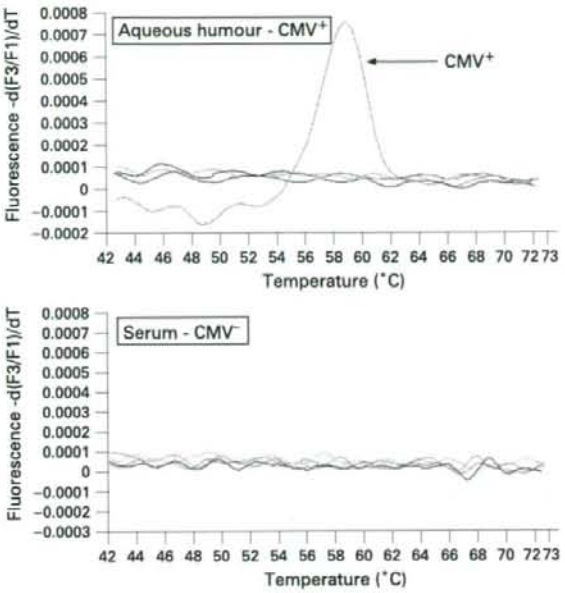

Figure 2 Results for a multiplex PCR in a patient with anterior uveitis. At 58°C, a significant positive curve was seen, indicating the detection of cytomegalovirus (CMV) genomic DNA in the aqueous humour. The other herpes viruses, such as herpes simplex virus (HSV) 1, HSV2, Varicella-zoster virus, Epstein–Barr virus, human herpes virus (HHV6), HHV7 and HHV8, were found to be negative in this particular sample. In addition, CMV-DNA was not detected in the patient's serum.

with several of them reported as being useful in the detection of herpes viruses when various combinations are employed.[7 18 19] In the current study, we were able to rapidly screen for the detection of the virus genome of all eight types of human herpes viruses by using several different primer pairs. When positive results were noted, we then used real-time quantitative PCR to examine the viral load using different primer pairs. This allowed us to confirm our positive results through the use of two PCR combinations.

It is important to discuss the significance of the high viral load of HHV in these patients. The finding of high viral loads in the ocular fluids indicates that virus replication takes place in the eye, suggesting a direct pathogenic role in intraocular inflammation. In the current study, some patients had previously been on systemic or topical corticosteroids over long periods of times before we collected the ocular samples. Therefore, we have to consider that long-term usage of topical and/or systemic steroids might be responsible for the creation of a steroid reservoir that could lead to a localised immunosuppressed state, thereby resulting in HHV replication. In order to be able to avoid the irreversible tissue damage and visual impairment caused by the viral infection, early treatment with anti-viral agents is clinically important, and this can be achieved if there is a rapid and accurate diagnosis of the viral infection in ocular tissues by PCR.

In summary, the HHV family-DNA was detected by multiplex PCR in the ocular fluids of patients with various types of uveitis. Among the positive samples that were identified through the use of qualitative PCR, many of these samples showed significantly high copy numbers of HHV-DNA, when examined by real-time PCR. However, it should be noted that

levels of the viral load for some of the intraocular samples could not be detected, for example, as was seen for the real-time PCR measurement of EBV. Thus, a qualitative multiplex PCR might be a useful method for screening viral infections, and furthermore, quantitative real-time PCR might make it possible to evaluate the clinical relevance of virus infections.

Acknowledgements: We would like to thank S Horie and Y Futagami, for their technical assistance. This work was supported by a Grant-in-Aid for Young Scientists (B) 18791263 of the Ministry of Education, Culture, Sports, Science and Technology, Japan.

Competing interests: None.

Ethics approval: The research followed the tenets of the Declaration of Helsinki, and all study protocols were approved by the Institutional Ethics Committees of Tokyo Medical and Dental University.

Patient consent: Informed consent was obtained from each patient prior to sample collection.

REFERENCES

1. **Ohashi Y,** Yamamoto S, Nishida K, *et al*. Demonstration of herpes simplex virus DNA in idiopathic corneal endotheliopathy. *Am J Ophthalmol* 1991;**112**:419–23.
2. **Yamamoto S,** Tada R, Shimomura Y, *et al*. Detecting varicella-zoster virus DNA in iridocyclitis using polymerase chain reaction. *Arch Ophthalmol* 1995;**113**:1358–9.
3. **Nakamura N,** Tanabe M, Yamada Y, *et al*. Zoster sine herpete with bilateral ocular involvement. *Am J Ophthalmol* 2000;**129**:809–10.
4. **Koizumi N,** Yamasaki K, Kawasaki S, *et al*. Cytomegalovirus in aqueous humor from an eye with corneal endotheliitis. *Am J Ophthalmol* 2006;**141**:564–5.
5. **Arimura E,** Deai T, Maruyama K, *et al*. Herpes simplex virus-2 quantification by real-time polymerase chain reaction in acute retinal necrosis. *Jpn J Ophthalmol* 2005;**49**:64–5.
6. **Asano S,** Yoshikawa T, Kimura H, *et al*. Monitoring herpesvirus DNA in three cases of acute retinal necrosis by real-time PCR. *J Clin Virol* 2004;**29**:206–9.
7. **Chichili GR,** Athmanathan S, Farhatullah S, *et al*. Multiplex polymerase chain reaction for the detection of herpes simplex virus, varicella-zoster virus and cytomegalovirus in ocular specimens. *Curr Eye Res* 2003;**27**:85–90.
8. **Sugita S,** Iwanaga Y, Kawaguchi T, *et al*. Detection of herpesviruses genome by multiplex PCR and real-time PCR in ocular fluids of patients with acute retinal necrosis [in Japanese]. *Nippon Ganka Gakkai Zasshi* 2008;**112**:30–8.
9. **Corey L,** Huang ML, Selke S, *et al*. Differentiation of herpes simplex virus types 1 and 2 in clinical samples by a real-time taqman PCR assay. *J Med Virol* 2005;**76**:350–5.
10. **Kimura H,** Morita M, Yabuta Y, *et al*. Quantitative analysis of Epstein–Barr virus load by using a real-time PCR assay. *J Clin Microbiol* 1999;**37**:132–6.
11. **Gautheret-Dejean A,** Manichanh C, Thien-Ah-Koon F, *et al*. Development of a real-time polymerase chain reaction assay for the diagnosis of human herpesvirus-6 infection and application to bone marrow transplant patients. *J Virol Meth* 2002;**100**:27–35.
12. **Hara S,** Kimura H, Hoshino Y, *et al*. Detection of herpesvirus DNA in the serum of immunocompetent children. *Microbiol Immnol* 2002;**46**:177–80.
13. **Polstra AM,** van den Burg R, Goudsmit J, *et al*. Human herpesvirus 8 load in matched serum and plasma samples of patients with AIDS-associated Kaposi's sarcoma. *J Clin Microbiol* 2003;**41**:5488–91.
14. **Kido S,** Sugita S, Horie S, *et al*. Association of varicella-zoster virus (VZV) load in the aqueous humor with clinical manifestations of anterior uveitis in herpes zoster ophthalmicus and zoster sine herpete. *Br J Ophthalmol* 2008;**92**:505–8.
15. **Takahashi H,** Sugita S, Shimizu N, *et al*. A high viral load of Epstein–Barr virus (EBV) DNA in ocular fluids in a HLA-B27 negative acute anterior uveitis patient with psoriasis. *Jpn J Ophthalmol*. In press.
16. **Kawaguchi T,** Sugita S, Shimizu N, *et al*. Kinetics of aqueous flare, intraocular pressure and virus-DNA copies in a patient with cytomegalovirus iridocyclitis without retinitis. *Inter Ophthalmol* 2007;**27**:383–6.
17. **Sugita S,** Shimizu N, Kawaguchi T, *et al*. Identification of human herpesvirus 6 in a patient with severe unilateral panuveitis. *Arch Ophthalmol* 2007;**125**:1426–7.
18. **Elnifro EM,** Cooper RJ, Klapper PE, *et al*. Multiplex polymerase chain reaction for diagnosis of viral and chlamydial keratoconjunctivitis. *Invest Ophthalmol Vis Sci* 2000;**41**:1818–22.
19. **Druce J,** Catton M, Chibo D, *et al*. Utility of a multiplex PCR assay for detecting herpesvirus DNA in clinical samples. *J Clin Microbiol* 2002;**40**:1728–32.

A New Humanized Mouse Model of Epstein-Barr Virus Infection That Reproduces Persistent Infection, Lymphoproliferative Disorder, and Cell-Mediated and Humoral Immune Responses

Misako Yajima,[1,a] Ken-Ichi Imadome,[1,a] Atsuko Nakagawa,[2] Satoru Watanabe,[3] Kazuo Terashima,[4] Hiroyuki Nakamura,[1] Mamoru Ito,[6] Norio Shimizu,[3] Mitsuo Honda,[5] Naoki Yamamoto,[4,5] and Shigeyoshi Fujiwara[1]

[1]Department of Infectious Diseases, National Research Institute for Child Health and Development, [2]Pathology Laboratory, Department of Clinical Laboratory Medicine, National Center for Child Health and Development, [3]Department of Virology, Division of Medical Science, Medical Research Institute, and [4]Department of Molecular Virology, Graduate School of Medicine, Tokyo Medical and Dental University, and [5]AIDS Research Center, National Institute of Infectious Diseases, Tokyo, and [6]Central Institute for Experimental Animals, Kawasaki, Japan

The functional human immune system, including T, B, and natural killer lymphocytes, is reconstituted in NOD/Shi-*scid*/IL-2Rγ^{null} (NOG) mice that receive hematopoietic stem cell transplants. Here, we show that these humanized mice can recapitulate key aspects of Epstein-Barr virus (EBV) infection in humans. Inoculation with $\sim 1 \times 10^3$ TD_{50} (50% transforming dose) of EBV caused B cell lymphoproliferative disorder, with histopathological findings and latent EBV gene expression remarkably similar to that in immunocompromised patients. Inoculation with a low dose of virus ($\leqq 1 \times 10^1$ TD_{50}), in contrast, resulted in apparently asymptomatic persistent infection. Levels of activated $CD8^+$ T cells increased dramatically in the peripheral blood of infected mice, and enzyme-linked immunospot assay and flow cytometry demonstrated an EBV-specific T cell response. Immunoglobulin M antibody specific to the EBV-encoded protein BFRF3 was detected in serum from infected mice. The NOG mouse is the most comprehensive small-animal model of EBV infection described to date and should facilitate studies of the pathogenesis, prevention, and treatment of EBV infection.

Epstein-Barr virus (EBV) is a tumor virus associated with a variety of malignancies, including Burkitt lymphoma, nasopharyngeal carcinoma, and Hodgkin lymphoma [1]. It is also an etiological agent of infectious mononucleosis (IM), which is characterized by transient proliferation of EBV-infected B lymphoblastoid cells and an excessive anti-EBV T cell response. EBV has a unique ability to growth transform human B lymphocytes in vitro and establish lymphoblastoid cell lines (LCLs) [2]. EBV-transformed lymphoblasts express 6 nuclear proteins (Epstein-Barr nuclear antigen [EBNA] 1, 2, 3A, 3B, 3C, and LP) and 3 membrane proteins (latent membrane protein [LMP] 1, 2A, and 2B), and this pattern of EBV gene expression is termed latency III. In contrast, Burkitt lymphoma cells express only EBNA1 consistently (latency I), whereas Hodgkin lymphoma and nasopharyngeal carcinoma cells express EBNA1, LMP1, and LMP2 (latency II). In vivo, EBV-transformed cells are effectively removed by virus-specific cytotoxic T cells, and EBV infection in immunocompetent humans is usually subclinical, except for IM caused by primary infection during adolescence or adulthood. However, in immunocompromised hosts, such as patients with AIDS and transplant recipients, EBV-infected B lymphoblasts can proliferate and cause lymphoproliferative disorder.

Received 28 December 2007; accepted 19 March 2008; electronically published 15 July 2008.

Potential conflicts of interest: none reported.

Financial support: Ministry of Health, Labour, and Welfare of Japan (grants H18-Shinko-013 and H19-AIDS-003).

[a] M.Y. and K.-I.I. contributed equally to this study.

Reprints or correspondence: Dr. Shigeyoshi Fujiwara, Dept. of Infectious Diseases, National Research Institute for Child Health and Development, 2-10-1 Okura, Setagaya-ku, Tokyo 157-8535, Japan (shige@nch.go.jp); or, Dr. Norio Shimizu, Dept. of Virology, Div. of Medical Science, Medical Research Institute, Tokyo Medical and Dental University, 1-5-45 Yushima, Bunkyo-ku, Tokyo 113-8519, Japan (nshivir@tmd.ac.jp); or, Dr. Naoki Yamamoto, AIDS Research Center, National Institute of Infectious Diseases, 1-23-1 Toyama, Shinjuku-ku, Tokyo 162-8640, Japan (nyama@nih.go.jp).

The Journal of Infectious Diseases 2008; 198:673–82

0022-1899/2008/19805-0008$15.00

DOI: 10.1086/590502

EBV infects only humans in nature and limited animal species under experimental conditions. It can infect cotton-top tamarins and induce lymphomas, which have been used as a model of EBV-associated lymphomas [3, 4]. Nonhuman primates possess their own lymphocryptoviruses related to EBV, and research on the use of these virus-host systems as models of EBV infection is currently in progress [5, 6]. Small-animal models of EBV have also been developed, which are particularly useful when a large number of animals are necessary. *Scid* mice that receive intraperitoneal transplants of EBV-transformed LCLs or peripheral blood mononuclear cells (PBMCs) isolated from EBV-infected persons develop lymphomas, which have been used as a model of human lymphoproliferative disorder [7–9]. Recently, NOD/*scid* mice transplanted with human hematopoietic stem cells (HSCs) and reconstituted mainly with B lymphocytes were infected with EBV, and the development of lymphoproliferative disorder was described [10]. The immune response to EBV was not studied in these *scid* or NOD/*scid* mouse models. Very recently, a functional human immune system could be reconstituted in highly immunodeficient mouse strains, and these so-called humanized mice were shown able to mount an EBV-specific T cell response [11, 12]. These studies were, however, performed mainly using immunological standpoints and did not provide detailed virological data.

NOD/Shi-*scid*/IL-2Rγ^{null} (referred to here as NOG) is a highly immunodeficient mouse strain that was developed very recently and that, after transplantation with cord blood HSCs, is able to reconstitute most major components of the hematolymphoid system, including T cells, B cells, NK cells, macrophages, and dendritic cells [13–15]. Human T cells that develop in NOG mice are functional in that they can be activated to display cytotoxic activity [15, 16]. These properties made NOG mice an excellent model of human virus infections targeting the immune system, such as those with human T-lymphotropic virus–1 and HIV-1 [17–20]. Here, we provide evidence that humanized NOG mice can reproduce various key aspects of human EBV infection and propose that they may be a valuable tool for studies of EBV infection.

METHODS

Preparation of humanized mice. NOG mice were obtained from the Central Institute for Experimental Animals (Kawasaki, Japan). Protocols for experiments with NOG mice were approved by the Institutional Animal Care and Use Committee of the National Institute of Infectious Diseases (NIID). Cord blood was supplied by the Tokyo Cord Blood Bank after obtaining informed consent. The use of human materials in this research was approved by the institutional review boards of the National Research Institute for Child Health and Development, the NIID, the Tokyo Medical and Dental University, and the Tokyo Cord Blood Bank. The isolation of human CD34$^+$ HSCs from cord blood by means of the MACS Direct CD34 Progenitor Cell Isolation Kit (Miltenyi Biotec), their intravenous injection (1×10^4 to 1.2×10^5 cells/mouse) into 6–10-week-old female NOG mice, and the characterization of the reconstitution of the human hematoimmune system were done as described elsewhere [18, 20]. NOG mice in which the human hematoimmune system was reconstituted are referred here as humanized NOG (hNOG) mice.

Experimental EBV infection, quantification of viral DNA, and detection of viral mRNAs. Virus production by EBV-infected Akata cells was stimulated by brief treatment with anti-IgG antibody (Dako), and culture fluid was used as inoculum after filtration through a 0.45-μm membrane filter [21]. For virus titration, cord blood lymphocytes were plated at the density

Table 1. Primers for reverse-transcription polymerase chain reaction to detect Epstein-Barr virus (EBV) transcripts.

Transcript, primer	Sequence (5′→3′)
EBNA1	
5′	gatgagcgtttgggagagctgattctgca
3′	tcctcgtccatggttatcac
EBNA2	
5′	agaggaggtggtaagcggttc
3′	tgacgggtttccaagactatcc
LMP1	
5′	ctctccttctcctcctcttg
3′	caggagggtgatcatcagta
LMP2A	
5′	atgactcatctcaacacata
3′	catgttaggcaaattgcaaa
LMP2B	
5′	cagtgtaatctgcacaaaga
3′	catgttaggcaaattgcaaa
EBER1	
5′	agcacctacgctgccctaga
3′	aaaacatgcggaccaccagc
BZLF1 (first)	
5′	attgcaccttgccgccaccttg
3′	cgcattttctggaagccacccga
BZLF1 (second)	
5′	gaccaagctaccagagtctat
3′	cagaatcgcattcctccagcga
BMRF1	
5′	ctagccgtcctgtccaagtgc
3′	agccaaacagctccttgccca
BLLF1	
5′	gtcagtacaccatccagagcc
3′	ttggtagacagccttcgtatg
GAPDH	
5′	gcctcctgcaccaccaactg
3′	cgacgcctgcttcaccaccctct

NOTE. EBNA, Epstein-Barr nuclear antigen; EBER, EBV-encoded small RNA; LMP, latent membrane protein.

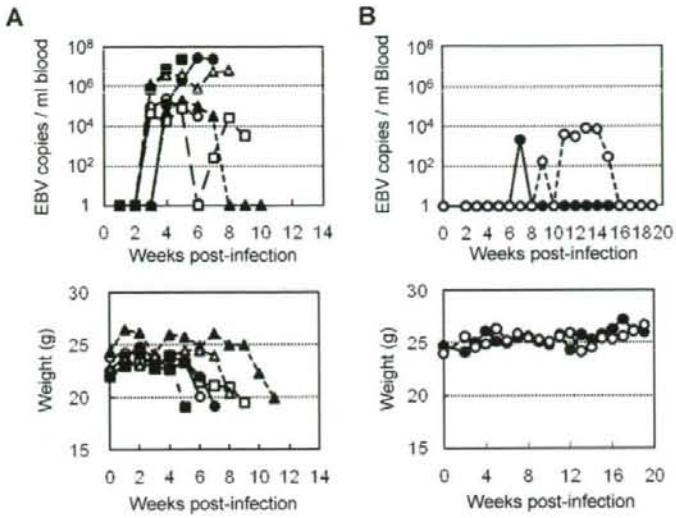

Figure 1. Peripheral blood Epstein-Barr virus (EBV) DNA load and body weight in humanized NOG (hNOG) mice infected with EBV. *A*, Infection at a high dose of virus. Six mice were inoculated intravenously with 1×10^3 TD_{50} of EBV. Peripheral blood EBV DNA load *(upper panels)* and body weight *(lower panels)* were then determined weekly. Each symbol in the graphs represents an individual mouse. Interruption of records indicates the death or killing of a mouse. *B*, Infection at lower doses. Peripheral blood EBV DNA load *(upper panel)* and body weight *(lower panel)* of 2 mice inoculated with low doses of EBV (*black circle*, 1×10^{-1} TD_{50}; *white circle*, 1×10^1 TD_{50}) are shown.

of 2×10^5 cells per well in 6-well plates and then inoculated with serial 10-fold dilutions of virus preparation. The number of wells with proliferating lymphocytes was counted 6 weeks after infection, and the titer of the virus in 50% transforming dose (TD_{50}) was determined by the Reed-Muench method [22]. EBV was inoculated intravenously through the tail vein. EBV DNA was quantified by a real-time quantitative polymerase chain reaction (PCR) assay based on the TaqMan system (Applied Biosystems), as described elsewhere [23]. Analysis of EBV gene expression by reverse-transcription PCR (RT-PCR) was done as described elsewhere, using the primers listed in table 1 [24].

Histopathology, in situ hybridization (ISH), and immunohistochemistry. Tissue samples were fixed in 10% buffered formalin, embedded in paraffin, and stained with hematoxylin-eosin. For phenotypic analysis of proliferating lymphocytes, immunostaining for CD3 (Nichirei), CD4 (Novocastra), CD8 (Nichirei), CD45RO, CD20, CD79a, CD30, Mum1 (Dako), CD23, CD10, CD56 (Novocastra), granzyme B (Dako), and T cell intracellular antigen 1 (Beckman Coulter) was performed on paraffin sections. EBV was detected by immunostaining for LMP1 and EBNA2 (Dako) and by ISH with EBV-encoded small RNA (EBER) probe. Immunohistochemistry and ISH were performed on an automated stainer (Benchmark XT; Ventana Medical Systems), in accordance with the manufacturer's recommendations. To determine the cell lineage of EBV-infected cells, paraffin sections were applied to double staining with EBER ISH and immunohistochemistry.

Detection of EBV-specific T cell response. Enzyme-linked immunospot (ELISPOT) assay was performed with the Immunocyto IFN-γ ELISPOT Kit (MBL), in accordance with the instructions supplied by the manufacturer. Briefly, $CD8^+$ T cells were isolated from PBMCs from EBV-infected hNOG mice with the IMag anti-human CD8 Particles–DM (BD Biosciences). Mixture of these $CD8^+$ T cells and an autologous LCL were incubated with interleukin (IL)–2 in microplates coated with antibody to interferon (IFN)–γ for 17 h. Captured IFN-γ was detected by use of biotinated antibody to IFN-γ and alkaline phosphatase–conjugated streptavidin and was visualized by reaction with the BCIP/NBT chromogen substrate. The unpaired Student's *t* test was used for statistical analysis. IFN-γ secretion in response to EBV was also examined by flow cytometry, as described elsewhere [25]. Briefly, aliquots of murine splenocytes and an LCL were mixed in 6-well plates in the presence of brefeldin A (10 μg/mL) and incubated at 37°C in 5% CO_2 for 17 h. After incubation, the cell suspensions were stained with phycoerythrin-conjugated anti-human CD69, phycoerythrin–Texas red–conjugated anti-human CD45, and phycoerythrin–cyanin 5–conjugated anti-human CD8 for 30 min at 4°C and were fixed with 2% paraformaldehyde. Cells were then permeabilized and stained with BD Perm/Wash buffer (BD Biosciences) containing fluorescein isothiocyanate–conjugated anti-human IFN-γ for 30 min at 4°C. Stained cells were analyzed using an EpicsXL flow cytometer (Beckman Coulter).

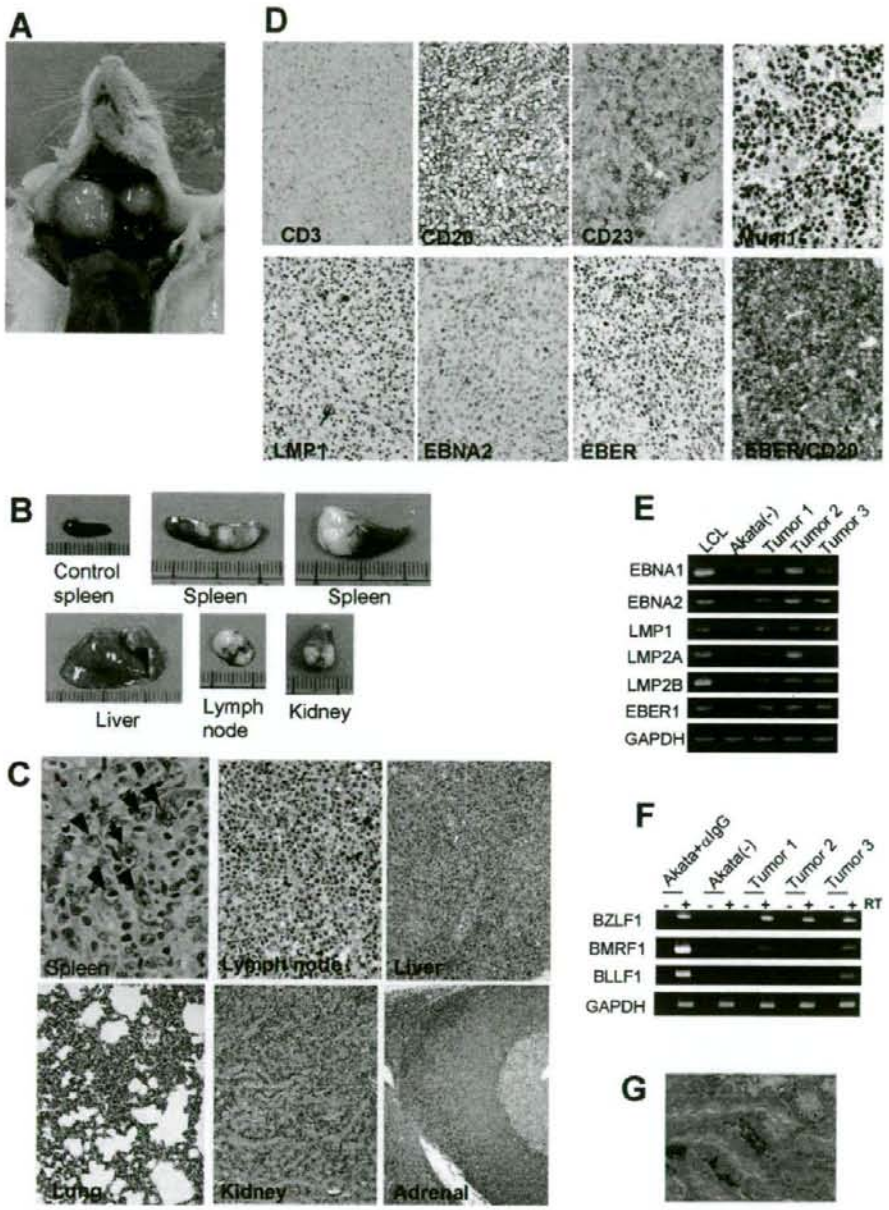

Figure 2. Pathological and virological analyses of Epstein-Barr virus (EBV)–infected humanized NOG (hNOG) mice. *A*, Photograph of an EBV-infected mouse showing tumors in the cervical area. *B*, Photographs of spleens, liver, lymph node, and kidney from EBV-infected mice with lymphoproliferative disorder. The upper left panel shows the spleen from an uninfected mouse. *C*, Photomicrographs of hematoxylin-eosin–stained tissues from mice with lymphoproliferative disorder. The arrow indicates a Reed-Sternberg–like cell, and the arrowheads indicate Hodgkin-like cells. Original magnifications, ×1000 for spleen, ×400 for lymph node, and ×200 for liver, lung, kidney, and adrenal gland. *D*, Immunohistochemical staining for lymphocyte surface markers (CD3, CD20, CD23, and Mum1) and EBV-encoded proteins (latent membrane protein [LMP] 1 and Epstein-Barr nuclear antigen [EBNA] 2), as well as in situ hybridization for EBV-encoded small RNA (EBER), in a lymph node from a mouse with lymphoproliferative disorder. The bottom right panel represents double staining for EBER and CD20. Original magnifications, ×200 for all except EBER/CD20, which is ×400. *E* and *F*, Reverse-transcription polymerase chain reaction detection of latent-cycle *(E)* and lytic-cycle *(F)* EBV gene expression in tumors from EBV-infected hNOG mice. Spleen tumors from 3 different mice were examined for the expression of EBNA1, EBNA2, LMP1, LMP2A, LMP2B, EBER1, BZLF1, BMRF1, and BLLF1. RNA samples from a lymphoblastoid cell line (LCL) *(E)* and anti-IgG–treated Akata cells *(F)* were used as positive controls, and an RNA sample from EBV-negative Akata cells (*E* and *F*) was used as a negative control. Assays were done with (+) or without (−) reverse transcriptase (RT) in panel F. Expression of GAPDH was examined as a reference. *G*, Double staining of EBER and CD20 in the liver of an hNOG mouse that was persistently infected with EBV without developing lymphoproliferative disorder. EBER is stained navy in the nucleus, and CD20 is stained brown in the membrane. Original magnification, ×1000.

Table 2. Quantification of Epstein-Barr virus (EBV) DNA in persistently infected humanized NOG mice.

Organ	Mouse	
	N35-1[a]	N35-3[b]
Bone marrow	ND	4.1×10^4
Spleen	6.2×10^2	5.7×10^3
Liver	ND	2.7×10^4
Lymph node (neck)	1.6×10^3	6.9×10^3
Lymph node (axilla)	ND	2.6×10^2
Lymph node (mesentery)	ND	4.1×10^2
Lungs	2.7×10^3	1.0×10^4
Kidneys	1.2×10^3	4.8×10^4
Adrenal gland	4.4×10^1	8.0×10^5

NOTE. Data are the amounts of EBV DNA measured 22 weeks after infection, in copies per microgram of DNA. ND, not detectable.

[a] Infected at 1×10^1 TD_{50}.

[b] Infected at 1×10^1 TD_{50}.

Detection of antibodies specific to EBV. IgM antibody to the EBV BFRF3 protein was detected by immunoblotting essentially as described elsewhere [24], except that horseradish peroxidase–conjugated antibody specific to human IgM (Beckman Coulter) was used as secondary antibody. To prepare the glutathione *s*-transferase (GST)–BFRF3 fusion protein, a DNA fragment spanning the entire coding region of BFRF3 was amplified by PCR (sense primer, 5'-GGCTCGAATTCATGGCACGCCG-GCTGCCC-3'; antisense primer, 5'-GGCTCGGATCCATAC-ACCATGTTTCGTGCCC-3') and inserted to the GST fusion vector pSGENT2, to yield the plasmid pSGENT2-BFRF3. *Escherichia coli* cells harboring pSGENT2-BFRF3 were stimulated with isopropyl β-D-1-thiogalactopyranoside to induce the expression of GST-BFRF3, which was subsequently purified by use of the Bulk GST Purification Module (GE Healthcare).

RESULTS

EBV infection in hNOG mice. Transplantation of human $CD34^+$ HSCs in NOG mice and reconstitution of the human hematoimmune system were done as described elsewhere [18, 20]. In the initial attempts at infection, 1×10^3 TD_{50} of the Akata strain of EBV was inoculated into 6 hNOG mice, and EBV DNA was demonstrated in the peripheral blood of all of them (figure 1*A*). EBV DNA was first evident at 3–4 weeks after inoculation and reached peak levels of $\sim 1 \times 10^6$ EBV DNA copies/μg of DNA. All 6 mice became seriously ill between 5 and 10 weeks after inoculation, with signs of weight loss (figure 1*A*), general inactivity, and piloerection. In contrast, EBV DNA was not detected in the peripheral blood, bone marrow, thymus, spleen, lymph nodes, liver, kidneys, and lungs of 3 control NOG mice that were not transplanted with HSCs but were inoculated with the virus (data not shown). Similarly, no signs of EBV infection were observed in 3 control hNOG mice that were not inoculated with the virus (data not shown). In total, 43 NOG mice that had been humanized with HSCs from 9 different cord blood samples were inoculated with 1×10^3 TD_{50} of EBV, and in 38 of them the results were similar to those observed in the initial 6 mice, with high blood EBV load and severe deterioration in their general condition. Ten of them died and could not be examined further. The remaining 28 mice were killed, and signs of lymphoproliferative disorder were found at autopsy (see the below). These results demonstrate that hNOG mice can be infected with EBV, with a mostly fatal outcome at this virus dose.

EBV-induced lymphoproliferative disorder in hNOG mice. Autopsy of killed mice showed signs of lymphoproliferative disorder typically represented by an overt tumor in the spleen (figure 2*B*). In ~70% (20/28) of the mice autopsied, macroscopical signs of disseminated disease were found in the liver, lymph nodes, or kidneys (figure 2*A* and 2*B*). Seventeen mice were examined pathologically, and 15 of them showed typical histology of diffuse large B cell lymphoma, with remarkable similarity to the human lymphoproliferative disorder in the immunocompromised hosts (figure 2*C*). The tissues contained occasional immunoblasts, Reed-Sternberg–like cells, and Hodgkin-like cells (figure 2*C*). Marked infiltration of large transformed lymphoid cells was also demonstrated in liver, lymph nodes, kidneys, adrenal glands, and lungs (figure 2*C*). Real-time PCR detected high levels ($\sim 1 \times 10^5$ to $\sim 1 \times 10^6$ EBV DNA copies/μg of DNA) of EBV DNA in these organs, and the large transformed lymphoid cells were universally EBV positive by EBER ISH (figure 2*D*). Immunohistochemical analysis showed that the large transformed lymphoid cells were of the activated B cell phenotype, being reactive for CD20 and CD23 and not reactive for CD3 and CD10 (figure 2*D* and data not shown). They were also positive for Mum-1, a late- and postgerminal center cell marker. The EBER-positive cells were CD20-positive B cells (figure 2*D*), and no EBER-positive T cells were identified. Immunostaining revealed that most proliferating cells expressed EBNA2, whereas LMP1 was expressed in only a fraction of them (figure 2*D*). RT-PCR analysis of typical spleen tumors obtained from 3 different mice showed the expression of EBNA1, EBNA2, LMP1, LMP2A, LMP2B; and EBER, consistent with the latency III program of EBV gene expression (figure 2*E*). In addition, transcripts from lytic-cycle EBV genes, including BZLF1 (immediate-early), BMRF1 (early), and BLLF1 (late, encoding gp350/220), were identified (figure 2*F*).

Virus dose–dependent outcome of EBV infection in hNOG mice. To examine the influence of virus dose on the outcome of EBV infection, we inoculated serial dilutions of EBV preparation into 2 lots of hNOG mice, each consisting of 5 mice that had been humanized with the same HSC preparation. Consistent with the results described above, the 4 mice (2 from each lot) that received the higher doses (1×10^3 and 1×10^2 TD_{50}) of the

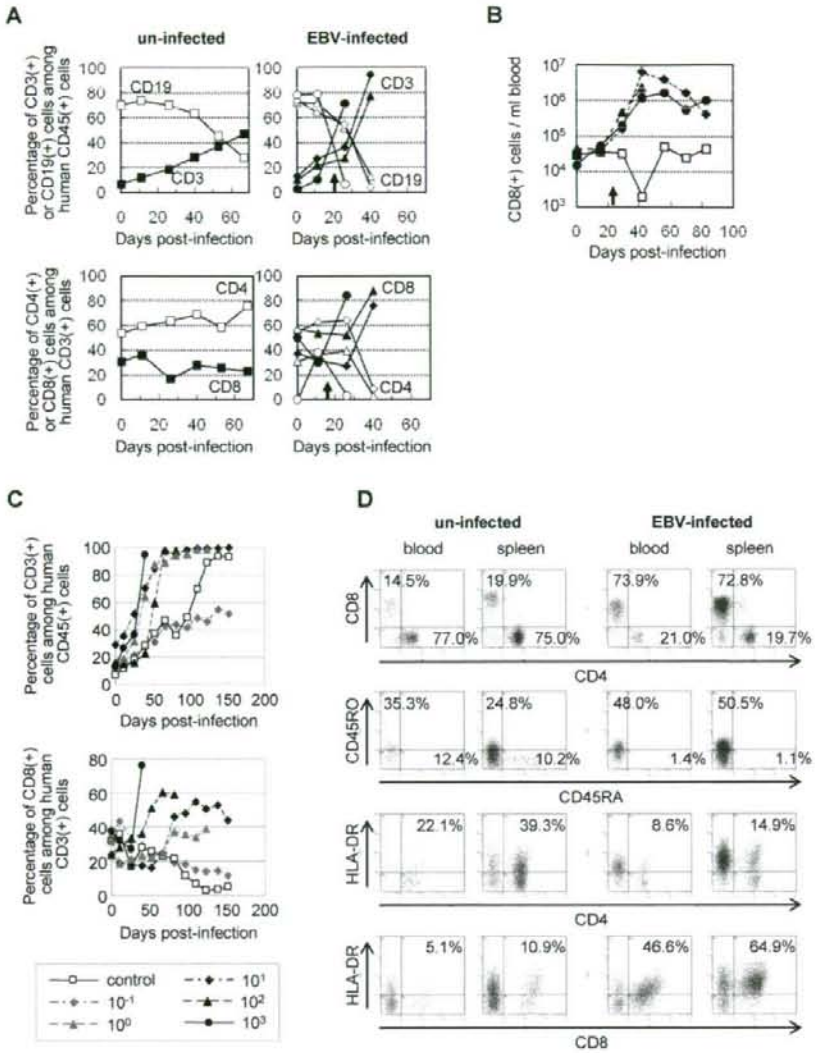

Figure 3. Surface marker expression by peripheral blood T cells in Epstein-Barr virus (EBV)–infected humanized NOG (hNOG) mice. *A*, Changes in the percentages of $CD3^+$ T cells and $CD19^+$ B cells among human $CD45^+$ leukocytes *(upper panels)* and in the percentages of $CD8^+$ cells and $CD4^+$ cells among $CD3^+$ cells *(lower panels)* after infection with EBV. Results obtained from 3 EBV-infected mice and an uninfected mice are shown. White symbols indicate the percentage of $CD19^+$ cells *(upper panels)* or $CD4^+$ cells *(lower panels)*; black symbols indicate the percentage of $CD3^+$ cells *(upper panels)* or $CD8^+$ cells *(lower panels)*. A vertical arrow in the graph area shows the time point at which EBV DNA was first detected in peripheral blood. *B*, Changes in the no. of $CD8^+$ T cells in the peripheral blood of EBV-infected hNOG mice. White symbols indicate uninfected mice, and black symbols indicate infected mice. Note that cell no. is plotted in a logarithmic scale. *C*, Viral dose–dependent T cell responses in hNOG mice inoculated with serially diluted EBV. Ten-fold serial dilutions of an EBV sample starting from 1×10^3 TD_{50} per inoculate were injected intravenously into NOG mice that had undergone transplantation with the same lot of human hematopoietic stem cells (HSCs). Changes in the percentages of $CD3^+$ T cells among human $CD45^+$ leukocytes *(upper panel)* and in the percentages of $CD8^+$ cells among $CD3^+$ cells *(lower panel)* after inoculation with EBV are shown. The viral dose for each mouse is shown in the key. *D*, Comparison of surface marker expression between EBV-infected mice and control mice. Two mice that underwent transplantation with the same lot of human HSCs were either inoculated with EBV or left uninfected; 10 weeks after inoculation, mononuclear cells obtained from peripheral blood or spleen were gated for the expression of human CD3 and then examined for the expression of CD8 and CD4 *(top panels)*, CD45RO and CD45RA *(second from top)*, HLA-DR and CD4 *(second from bottom)*, and HLA-DR and CD8 *(bottom)*.

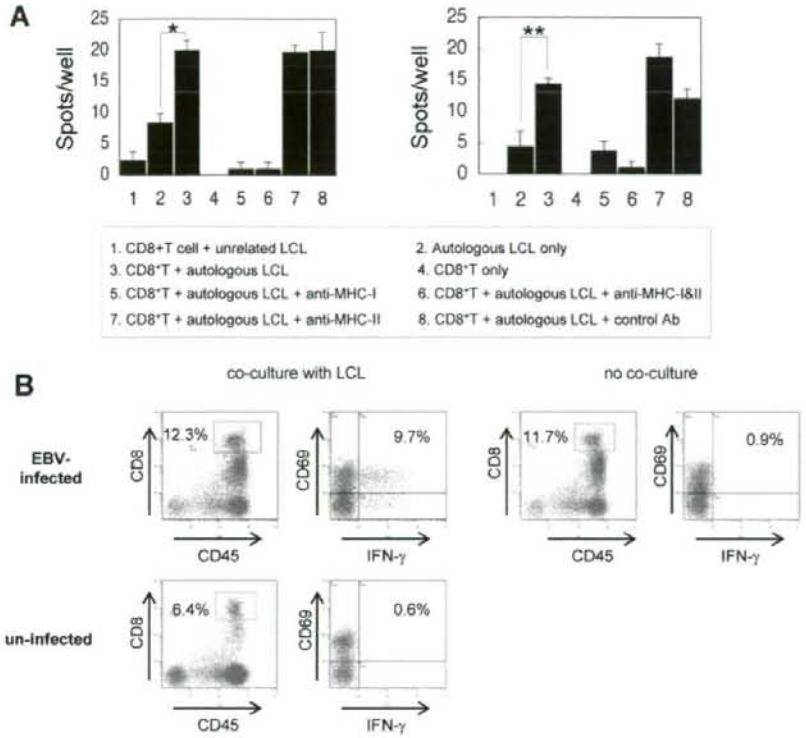

Figure 4. Epstein-Barr virus (EBV)–specific T cell response in humanized NOG (hNOG) mice. *A*, Enzyme-linked immunospot assay for the detection of human T cells producing interferon (IFN)–γ after stimulation with an EBV-positive lymphoblastoid cell line (LCL). $CD8^+$ cells isolated from EBV-infected hNOG mice were cocultured with an autologous LCL, and IFN-γ–secreting cells were counted (3, 5, 6, 7, and 8). To analyze restriction by major histocompatibility complex (MHC), antibody to HLA class I (anti–human HLA-ABC clone W6/32; eBioscience) (5), antibodies to both HLA class I and class II (6), antibody to HLA class II (anti–human HLA-DP,DQ,DR clone CR3/43; Dako) (7), or isotype-matched control antibody (8) were added to the culture. Control experiments included coculture of $CD8^+$ cells with an MHC-mismatched LCL (1), culture of the autologous LCL only (2), and culture of $CD8^+$ cells only (4). Results from 2 infected mice are shown. Five hundred $CD8^+$ cells per well were cultured in the experiment shown on the left, and 250 $CD8^+$ cells per well were cultured in that shown on the right. Spots were counted in triplicate in each of the 8 experimental groups, and the bars represent mean values and SEs. The unpaired Student's *t* test was used for statistical analysis. $^*P < .01$ and $^{**}P < .02$. *B*, Detection of human $CD8^+$ cells that produce IFN-γ in response to stimulation with an EBV-positive LCL by flow cytometry. $CD8^+$ cells were isolated from the spleen of an EBV-infected mouse and cocultured with the autologous LCL. Intracellular IFN-γ was stained and analyzed as described in Methods.

virus died of lymphoproliferative disorder ~5–10 weeks after inoculation. The remaining mice in both of the lots that received lower doses (1×10^1, 1×10^0, and 1×10^{-1} TD_{50}) survived acute infection and appeared normal throughout the observation period of 22 weeks. Although EBV DNA was detected at variable levels in their peripheral blood several weeks after inoculation, it returned to undetectable levels thereafter (figure 1*B*), suggesting that a certain protection mechanism worked to control EBV infection. Importantly, EBV DNA could be still detected in various organs, including spleen, liver, lungs, kidneys, and adrenal glands, at the end of the observation period (22 weeks), indicating that EBV persisted in these mice (table 2). Double staining for EBER and CD20 showed that EBV persisted in B cells (figure 2*G*). Macroscopical examination by autopsy at the end of the observation period did not reveal abnormality in these mice, except for moderate splenomegaly found in a mouse that received 1×10^1 TD_{50}. These results indicate that the outcome of EBV infection in hNOG mice varies with the virus dose; high doses of virus tend to cause fatal lymphoproliferative disorder, whereas lower doses induce apparently asymptomatic persistent infection.

EBV-specific T cell response in hNOG mice. Flow cytometry analysis demonstrated a dramatic increase in the percentage of $CD3^+$ T cells among the human $CD45^+$ leukocytes after infection with EBV. This increase in T cells was accompanied by an increase in the percentage of $CD8^+$ cells among human $CD3^+$ T cells. These changes were seen in virtually all infected mice, and the results from 3 mice are shown in figure 3*A*. The slow increase in the percentage of $CD3^+$ cells in the uninfected mouse represents the process of humanization (i.e., the development of hu-

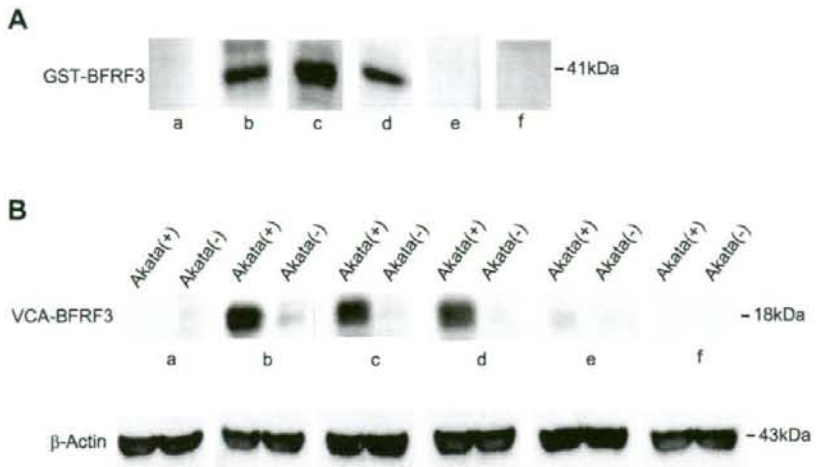

Figure 5. Demonstration of IgM antibody to the Epstein-Barr virus (EBV) BFRF3 protein in the serum of humanized NOG (hNOG) mice. *A*, Immunoblot with the glutathione *s*-transferase (GST)–BFRF3 fusion protein. Purified GST-BFRF3 fusion protein was examined with serum from an EBV-uninfected person *(a)*, an EBV-infected person *(b)*, EBV-infected hNOG mice (*c* and *d*), and an uninfected hNOG mice (*e* and *f*). *B*, Immunoblot with the lysate of EBV-producing Akata cells. Lysate of anti-IgG–treated Akata cells, labeled Akata(+), and of EBV-negative Akata cells, labeled Akata(−), was examined using serum from an EBV-uninfected person *(a)*, an EBV-infected person *(b)*, EBV-infected hNOG mice (*c* and *d*), and uninfected hNOG mice (*e* and *f*).

man T cells). This increase in $CD8^+$ cells were even more conspicuous when their definite number was counted (figure 3*B*). When hNOG mice were inoculated with serially diluted virus samples, a striking dose response was evident; mice inoculated with higher doses exhibited a more profound increase in $CD8^+$ cells at earlier time points (figure 3*C*). Further flow cytometry analyses showed that $CD45RO^+$ memory T cells, compared with $CD45RA^+$ T cells, increased in infected hNOG mice (figure 3*D*). Expression of a T cell activation marker, HLA-DR, was observed mainly in $CD8^+$ cells rather than in $CD4^+$ cells (figure 3*D*).

To demonstrate that these $CD8^+$ T cells were directed against EBV-infected cells, we examined IFN-γ secretion after stimulation with EBV-transformed cells. For this purpose, we first established an LCL using B cells isolated from the same cord blood that was used to isolate HSCs for transplantation. $CD8^+$ T cells, isolated from the peripheral blood of EBV-infected hNOG mice, were incubated with this autologous LCL, and cells secreting IFN-γ were detected by ELISPOT assay. For all 3 EBV-infected hNOG mice (which had been infected at 1×10^3 TD_{50}) thus examined, a significant number of spots were recognized in the wells in which $CD8^+$ T cells were mixed with the autologous LCL, whereas those cells incubated with unrelated LCL had many fewer spots (data from 2 mice are shown in figure 4*A*). $CD8^+$ T cells isolated from uninfected hNOG mice did not give a significant number of spots (data not shown). Release of IFN-γ was blocked by antibody specific to human major histocompatibility complex (MHC) class I but not by that specific to human MHC class II (figure 4*A*). These results clearly show that a T cell response restricted by human MHC class I was mounted against EBV-infected cells. In addition, in 5 of the 6 EBV-infected hNOG mice examined (infected at 1×10^3 TD_{50}), flow cytometry also demonstrated production of IFN-γ by $CD8^+$ T cells isolated from the spleen and stimulated with an autologous LCL (figure 4*B*).

EBV-specific antibody response in hNOG mice. Serum samples from 30 EBV-infected hNOG mice were examined by Western blotting for IgM antibodies reactive with a bacterially expressed GST-BFRF3 fusion protein. The BFRF3 protein is a major component of the virus capsid antigen of EBV [26]. The results are shown in figure 5*A* and indicated that four serum samples (from mice infected at 1×10^1 or 1×10^3 TD_{50}) contained IgM antibody reactive with it. These serum samples reacted also with the 18-kDa BFRF3-encoded protein in the lysate of Akata cells stimulated with IgG antibody to activate virus production (figure 5*B*). Similar experiments with human IgG–specific secondary antibody did not show a positive reaction with either GST-BFRF or $p18^{BFRF3}$. Six serum samples collected from uninfected hNOG mice reacted with neither the 18-kDa protein nor GST-BFRF3 (figure 5 and data not shown). These results indicate that hNOG mice have the ability to mount an IgM response to EBV.

DISCUSSION

The lymphoproliferative disease induced in hNOG mice is remarkably similar to the human lymphoproliferative disorder seen in immunocompromised hosts [27] with respect to histology, surface phenotype, and the type of EBV gene expression

(latency III). Reproduction of latency III in the present study makes for an interesting contrast with the previous model using NOD/*scid* mice, which exhibited the latency II pattern [10].

EBV infection in lower doses resulted in a transient increase in EBV DNA load in the peripheral blood, followed by apparently asymptomatic infection that persisted for at least 22 weeks. This type of asymptomatic EBV infection has not been described in nonprimate models of EBV infection and may be regarded as a model of human EBV latency. To compare this condition in NOG mice with EBV latency in humans precisely, we need to further investigate the nature of host cells (i.e., whether they are memory B cells), the pattern of EBV gene expression in them, and the involvement of anti-EBV immune responses in its maintenance.

In hNOG mice, human T cells develop in thymus tissue, in which epithelial cells are of murine origin [16]. It is therefore interesting that they could mount a T cell response restricted by human MHC class I. Although this suggests that positive selection of human T cells occurred in hNOG mice, the mechanism of T cell education remains unclear. Alloantigen-specific and human MHC class I–restricted T cell cytotoxicity has been reported in hNOG mice [15, 16]. An EBV-induced T cell response was evident in mice that received high doses of virus and developed lymphoproliferative disorder, suggesting that the T cell response in hNOG mice was not sufficient to control EBV-induced lymphoproliferation when they were infected at high doses. That only a minor fraction of $CD8^+$ T cells appeared to be EBV specific, as evidenced by ELISPOT assay and flow cytometry, may explain this result, at least partially. A humoral immune response to EBV has not been documented in previous mouse models of EBV infection, and therefore the NOG mouse may provide a valuable tool to analyze the mechanism and the protective roles of antibody response in EBV infection. We have to date clearly identified only IgM antibody to the 18-kDa component of virus capsid antigen in a minor fraction (4/30) of infected mice. We are currently attempting to improve sensitivity and to see whether hNOG mice can mount a more efficient and divergent antibody response to the virus, possibly including the production of IgG antibodies. Because both the T cell–mediated and the humoral immune response are elicited in hNOG mice, they may be useful in the evaluation of candidate EBV vaccines.

Very recently, humanized mice based on other immunodeficient mouse strains were prepared, and EBV was used as a typical pathogen to analyze their immune functions. Traggiai et al. [12] infected humanized $Rag2^{-/-}IL\text{-}2R\gamma^{-/-}$ mice with EBV and documented an in vitro proliferative response by $CD8^+$ T cells to an autologous LCL. Melkus et al. [11], on the other hand, humanized NOD/*scid* mice by transplanting human fetal liver, thymus, and HSCs and succeeded in inducing an EBV-specific T cell immune response as well as an innate immune response to toxic shock syndrome toxin 1. These 2 studies were performed mainly using immunological standpoints and did not provide detailed data from virological investigations. An advantage of the NOG mouse model described here is that it does not require a fine surgical procedure using human fetal tissue; therefore, NOG mice can be easily provided in large quantities.

In immunocompromised humans, failure of immunosurveillance may lead to the development of lymphoproliferative disorder. We expect that the NOG mouse model can be used to analyze the exact relationship between immunodeficiency and the development of lymphoproliferative disorder. Immune responses in the hNOG mouse can be modulated by immunosuppressive drugs (such as cyclosporine A) or HIV, and the development of lymphoproliferative disorder can be analyzed with special reference to the nature and level of immunodeficiency. This kind of study, which has not been possible with conventional *scid* mice, may reveal an exact condition in which lymphoproliferative disorder develops and may thereby aid the development of a specified immunosuppressive procedure that evades this condition and precludes the risk of lymphoproliferative disorder.

In summary, the NOG mouse is able to recapitulate various essential elements of human EBV infection and is therefore, to our knowledge, the most comprehensive small-animal model of EBV infection described to date. It should be a valuable tool for the study of the pathogenesis, prevention, and treatment of EBV infection.

Acknowledgments

We thank Satoshi Itakura, Fuyuko Kawano, Eri Yamada, Miki Mizukami, and Ken Watanabe for technical assistance. We thank Shizuko Minegishi for advice on flow cytometry, Atsushi Komano for advise on the enzyme-linked immunospot assay, Ayako Demachi-Okamura and Kiyotaka Kuzushima for advice on detection of Epstein-Barr virus–specific T cells, and Shosuke Imai for helpful discussions. We thank the Tokyo Cord Blood Bank for supplying cord blood.

References

1. Rickinson AB, Kieff E. Epstein-Barr virus. In: Knipe DM, Howley PM, eds. Fields virology. Philadelphia: Lippincott Williams & Wilkins, **2001**: 2575–628.
2. Kieff E, Rickinson AB. Epstein-Barr virus and its replication. In: Knipe DM, Howley PM, eds. Fields virology. 4th ed. Philadelphia: Lippincot Williams & Wilkins, **2001**:2511–74.
3. Young LS, Finerty S, Brooks L, Scullion F, Rickinson AB, Morgan AJ. Epstein-Barr virus gene expression in malignant lymphomas induced by experimental virus infection of cottontop tamarins. J Virol **1989**; 63: 1967–74.
4. Miller G, Shope T, Coope D, et al. Lymphoma in cotton-top marmosets after inoculation with Epstein-Barr virus: tumor incidence, histologic spectrum antibody responses, demonstration of viral DNA, and characterization of viruses. J Exp Med **1977**; 145:948–67.
5. Cho Y, Ramer J, Rivailler P, et al. An Epstein-Barr-related herpesvirus from marmoset lymphomas. Proc Natl Acad Sci USA **2001**; 98:1224–9.
6. Moghaddam A, Rosenzweig M, Lee-Parritz D, Annis B, Johnson RP, Wang F. An animal model for acute and persistent Epstein-Barr virus infection. Science **1997**; 276:2030–3.
7. Mosier DE, Gulizia RJ, Baird SM, Wilson DB. Transfer of a functional human immune system to mice with severe combined immunodeficiency. Nature **1988**; 335:256–9.

8. Okano M, Taguchi Y, Nakamine H, et al. Characterization of Epstein-Barr virus-induced lymphoproliferation derived from human peripheral blood mononuclear cells transferred to severe combined immunodeficient mice. Am J Pathol **1990**; 137:517–22.
9. Rowe M, Young LS, Crocker J, Stokes H, Henderson S, Rickinson AB. Epstein-Barr virus (EBV)-associated lymphoproliferative disease in the SCID mouse model: implications for the pathogenesis of EBV-positive lymphomas in man. J Exp Med **1991**; 173:147–58.
10. Islas-Ohlmayer M, Padgett-Thomas A, Domiati-Saad R, et al. Experimental infection of NOD/SCID mice reconstituted with human CD34+ cells with Epstein-Barr virus. J Virol **2004**; 78:13891–900.
11. Melkus MW, Estes JD, Padgett-Thomas A, et al. Humanized mice mount specific adaptive and innate immune responses to EBV and TSST-1. Nat Med **2006**; 12:1316–22.
12. Traggiai E, Chicha L, Mazzucchelli L, et al. Development of a human adaptive immune system in cord blood cell-transplanted mice. Science **2004**; 304:104–7.
13. Hiramatsu H, Nishikomori R, Heike T, et al. Complete reconstitution of human lymphocytes from cord blood CD34+ cells using the NOD/SCID/γ_c^{null} mice model. Blood **2003**; 102:873–80.
14. Ito M, Hiramatsu H, Kobayashi K, et al. NOD/SCID/γ_c^{null} mouse: an excellent recipient mouse model for engraftment of human cells. Blood **2002**; 100:3175–82.
15. Yahata T, Ando K, Nakamura Y, et al. Functional human T lymphocyte development from cord blood CD34+ cells in nonobese diabetic/Shi-scid, IL-2 receptor gamma null mice. J Immunol **2002**; 169:204–9.
16. Ishikawa F, Yasukawa M, Lyons B, et al. Development of functional human blood and immune systems in NOD/SCID/IL2 receptor γ chain^{null} mice. Blood **2005**; 106:1565–73.
17. Miyazato P, Yasunaga J, Taniguchi Y, Koyanagi Y, Mitsuya H, Matsuoka M. De novo human T-cell leukemia virus type 1 infection of human lymphocytes in NOD-SCID, common gamma-chain knockout mice. J Virol **2006**; 80:10683–91.
18. Watanabe S, Terashima K, Ohta S, et al. Hematopoietic stem cell-engrafted NOD/SCID/IL2Rgamma null mice develop human lymphoid systems and induce long-lasting HIV-1 infection with specific humoral immune responses. Blood **2007**; 109:212–8.
19. Dewan MZ, Terashima K, Taruishi M, et al. Rapid tumor formation of human T-cell leukemia virus type 1-infected cell lines in novel NOD-SCID/gammac^{null} mice: suppression by an inhibitor against NF-kappaB. J Virol **2003**; 77:5286–94.
20. Watanabe S, Ohta S, Yajima M, et al. Humanized NOD/SCID/IL2Rγ^{null} mice transplanted with hematopoietic stem cells under nonmyeloablative conditions show prolonged life spans and allow detailed analysis of human immunodeficiency virus type 1 pathogenesis. J Virol **2007**; 81: 13259–64.
21. Takada K, Ono Y. Synchronous and sequential activation of latently infected Epstein-Barr virus genomes. J Virol **1989**; 63:445–9.
22. Condit RC. Principles of virology. In: Knipe DM, Howley PM, eds. Fields virology. Philadelphia: Lippincott Williams & Wilkins, **2001**:19–51.
23. Kimura H, Morita M, Yabuta Y, et al. Quantitative analysis of Epstein-Barr virus load by using a real-time PCR assay. J Clin Microbiol **1999**; 37:132–6.
24. Nakamura H, Iwakiri D, Ono Y, Fujiwara S. Epstein-Barr-virus-infected human T-cell line with a unique pattern of viral-gene expression. Int J Cancer **1998**; 76:587–94.
25. Kuzushima K, Hoshino Y, Fujii K, et al. Rapid determination of Epstein-Barr virus-specific CD8$^+$ T-cell frequencies by flow cytometry. Blood **1999**; 94:3094–100.
26. van Grunsven WM, Nabbe A, Middeldorp JM. Identification and molecular characterization of two diagnostically relevant marker proteins of the Epstein-Barr virus capsid antigen complex. J Med Virol **1993**; 40: 161–9.
27. Rezk SA, Weiss LM. Epstein-Barr virus-associated lymphoproliferative disorders. Hum Pathol **2007**; 38:1293–304.